HUMAN FOREARM REHABILITATION AND MONITORING SYSTEMS

ADRIANA COMANESCU[1], MARIUS DINCA[2],
DORU BOBLEA[3], ANTONIA ONACA[4], ANDREEA NEAGOE[1]

Abstract. The human upper limb has a special anatomical complexity allowing for extraordinary mobility. Literature reports over 8 000 degrees of freedom in the hand alone [12–15] making an engineering marvel. It can be assimilated with a biorobot with open and closed chains that give exceptional functional mobility. Due to this complex structure, there are no specific solutions for human upper limb recovery systems in the existing literature. Based on the short anatomical details included in the paper [11–20], a simplified version of the human upper limb in the sagittal plane is created, which is necessary for designing its recovery and functional systems. This bi-mobile planar mechanism consists of three main segments corresponding to the humerus, forearm and palm. It is completed with a closed chain to simulate the palm, being attached to the sagittal model. A specific algorithm is used to obtain the model's positional-kinematic characteristics for standard anatomic details. The forearm also possesses a unique movement called pronation-supination, which allows it to rotate. This motion can be replicated using a spatial mechanism. By integrating these two mechanisms, a single system for use in medical rehabilitation, specifically designed to aid in the forearm functional recovery can be created.

Key words: bi-mobile mechanism, forearm sagittal model, pronation-supination model, positional -kinematic characteristics, model algorithm, inverse modelling, direct modelling.

1. HUMAN UPPER LIMB ANATOMICAL DETAILS

The main segments of the human upper limb are humerus, forearm and palm – hand having carpus, metacarpus and phalanges components (Fig. 1). The

[1] "Politehnica" University of Bucharest, Romania
[2] Active Life Therapy, Bucharest, Romania
[3] Atlantic Technological University, Galway, Ireland
[4] "Carol Davila" University of Medicine and Pharmacy, Bucharest, Romania

Ro. J. Techn. Sci. – Appl. Mechanics, Vol. 69, N^{os} 2–3, P. 139–156, Bucharest, 2024

DOI:10.59277/RJTS-AM.2024.2-3.03

forearm consists of two bones [11–18], which are in contact both in the upper and lower parts, the connections being mechanically equivalent to some higher kinematic pairs [12–18]. Between the radius and ulna a free space is created, called interosseous space (Fig. 2).

The radius is placed in continuation of the thumb and exceeds in length at its lower extremity, while the ulna through its inferior epiphysis. The inferior epiphysis of the radius is part of the radius-carpus joint.

The ulna is in the extension of the little finger and extends beyond the radius in the upper part through its upper epiphysis being part of the elbow joint.

The diaphysis of the radius or ulna is the portion located between the extremities – epiphyses – superior and inferior, and it has a triangular prismatic shape with three surfaces and three edges. More details for anatomical particularities [11–15] are given in Fig. 2.

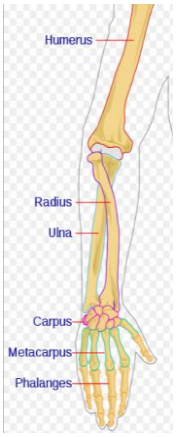

Fig. 1 – Upper limb anatomical details.

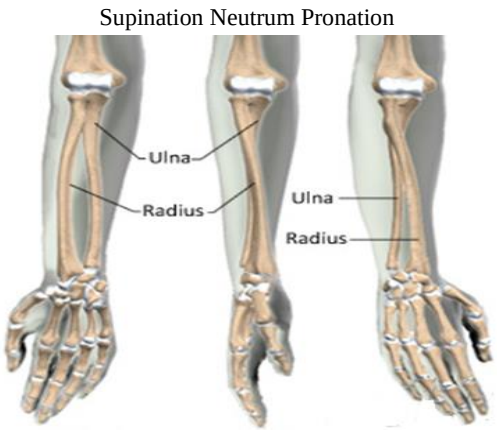

Fig. 2 – Functional particularities.

The characteristic elements of the radius – head, radius neck, radial tuberosity, radial margin and epiphysis with styloid process are shown in Fig. 3.

The head (Fig. 3a) is delimited at the top by a concave surface (Fig. 3b). The radial tuberosity (Fig. 3c) is an insertion point of the supinator muscle (Fig. 3f), which determines the mobility of the radius in relation to the humerus (Fig. 6).

The radial edge of the radius (Fig. 3d), is connected to the interosseous membrane located in the bony space with the ulna (Fig. 3e).

In the inferior epiphysis of the radius, the ulnar incision can be distinguished (Fig. 3g), which provides the connection with the ulna (Fig. 3h), this connection being a higher kinematic pair.

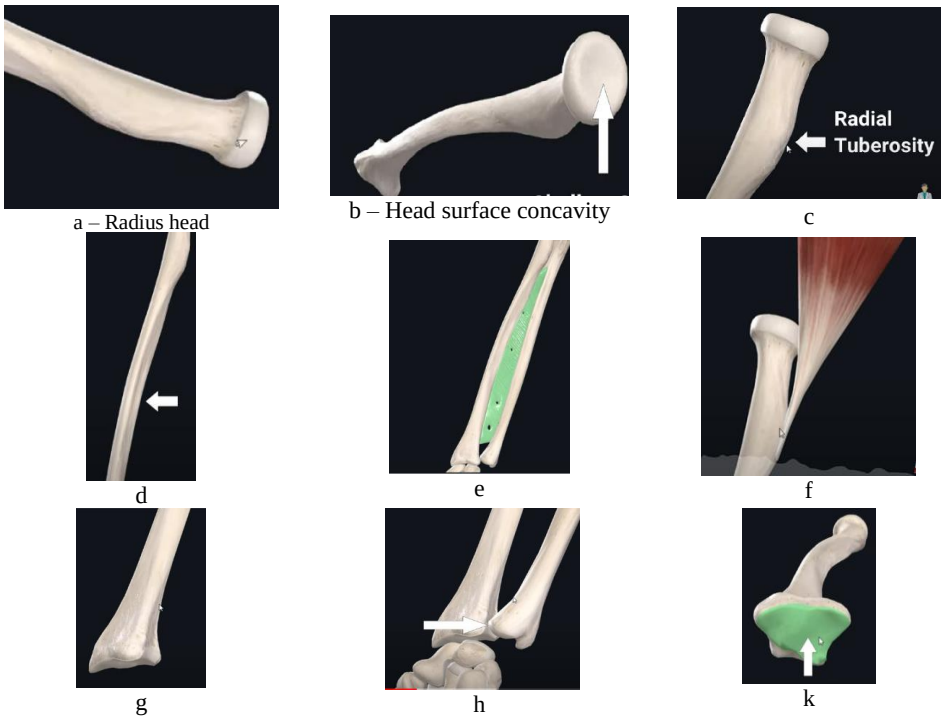

a – Radius head b – Head surface concavity c

d e f

g h k

Fig. 3 – Radius and ulna characteristics.

The carpal joint (Fig. 3k) is formed in the inferior epiphyseal area, determining the articulation of the lateral radius with the scaphoid (Fig. 4a), and median radius with the lunatus (Fig. 4b), which can also be equated with higher kinematic pairs. In the area of the superior epiphysis of the radius, its peripheral part articulates the interstitial space of the ulna (Fig. 5a), where it is placed the ligament connecting the radius to the ulna (Fig. 5b) and ensuring the contact of the two elements. This connection of the radius to the ulna is mechanically equivalent to a higher kinematic pair.

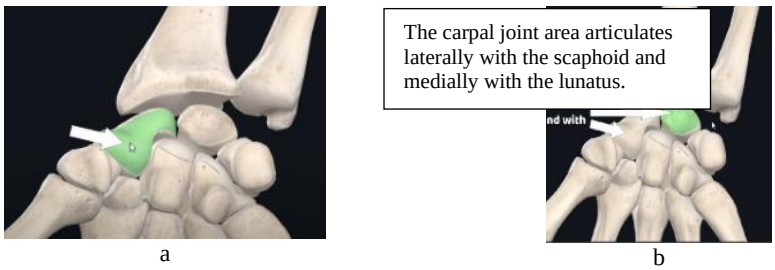

a b

Fig. 4 – The carpal joint.

a – the peripheral part of the radius articulates the ulna interstitial space.

b – the ligament connecting the radius to the ulna.

Fig. 5 – Radius superior epiphysis.

The mobility of the radius in relation to the humerus is shown in Fig. 6 and is due to the two muscles – supinator (Fig. 6a) and pronator (Fig. 6b).

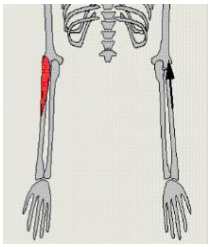

a – supinator

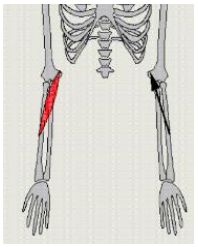

b – pronator

Fig. 6 – Radius relative mobility to humerus.

The elbow joint (Fig. 7) is a complex joint consisting of three bones, namely the humerus with its distal extremity, the radius and the ulna – ulna (with the proximal extremity). The ligaments of the elbow joint shown in Fig. 8 are also noteworthy [11–15].

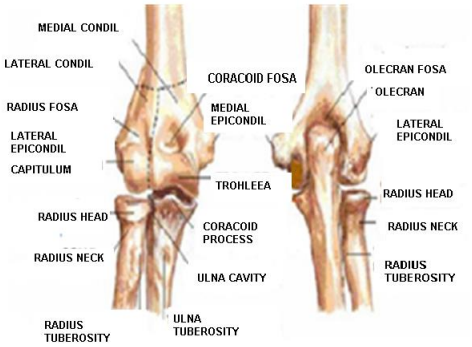

Fig. 7 – The elbow joint.

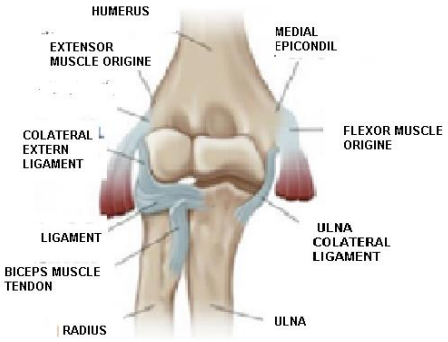

Fig. 8 – The elbow joint ligaments.

Thus, three joints specific to the elbow joint are distinguished, namely: the humerus-ulna joint (Fig. 9), mobile and uniaxial, and allowing the forearm to be balanced), the humerus-radius joint (Fig. 10), and the radius-ulna joint (Fig. 11), located in the lower part of the elbow joint and performing the pronation and supination movements of the forearm (Fig. 2).

Fig. 9 – Humerus-ulna joint.

Fig. 10 – Humerus-radius joint.

Fig. 11 – Radius-ulna joint.

2. HUMAN UPPER LIMB MODELS

Based on the anatomical details presented above, a simplified version of the human arm was made in the sagittal plane (Fig. 12), consisting of three characteristic components: humerus, forearm and palm (Fig. 1).

The three segments of the arm (Fig. 1 and Fig. 13) are articulated respectively in A (elbow joint) and C (palmar joint) the points O, B, G and F being the insertion points of some muscles, which ensure the mobility of segments in the sagittal plane. The origin of the chosen reference system lies at the D extremity of the middle finger, the vertical axis being coincident with the vertical position of the arm (Fig. 13).

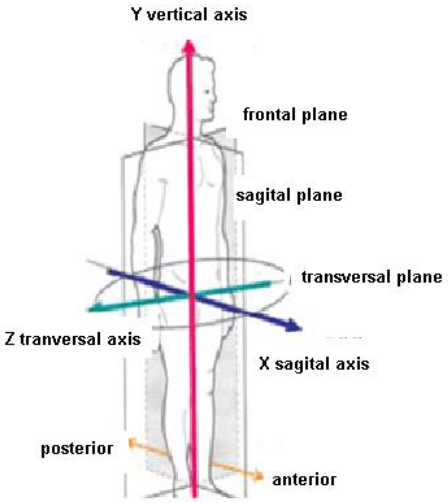

Fig. 12 – Human body principale plane.

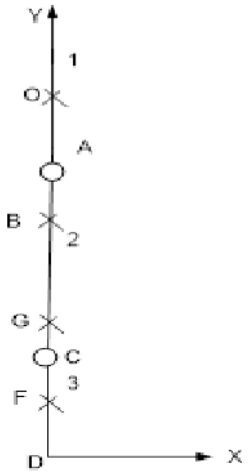

Fig. 13 – Upper limb sagittal view.

The angle of oscillation of the forearm (made through the ulna) in relation to the humerus is denoted as ϕ, and the angle of the hand in relation to the forearm as ψ (Fig. 14).

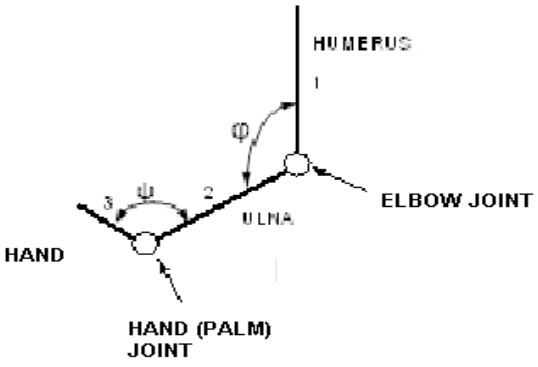

Fig. 14 – Forearm angular parameters.

The arm in the sagittal plane is a planar bi-mobile mechanism (Fig. 15a) with the active translation pairs respectively (4.5) and (6.7), which determine the variation of angles ϕ and ψ.

The mechanism is obtained from the only bi-mobile and bi-contour decomposable linkage (Fig. 15b), the same used in the structure of the classic Stewart foot [1–5].

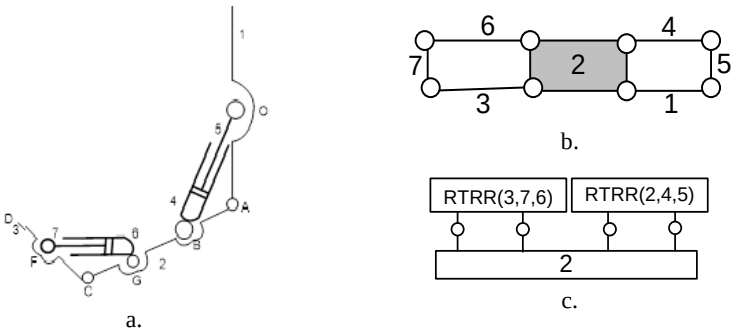

Fig. 15 – Structural sagittal model.

From a structural point of view, the mechanism consists of two active modular groups RTRR (Fig. 15c), the independent parameters being OB and GF respectively (Fig. 16).

The constant geometric parameters of the mechanism (Fig. 16) shown in Table 1 correspond to the standard proportion of arm element size.

Table 1

Arm standard element size

	Constant geometric parameters [mm]							
AC = LH	CD	CF	AB	AG	XA	YA	XO	YO
160	100	37.2	60	100	0	260	0	320

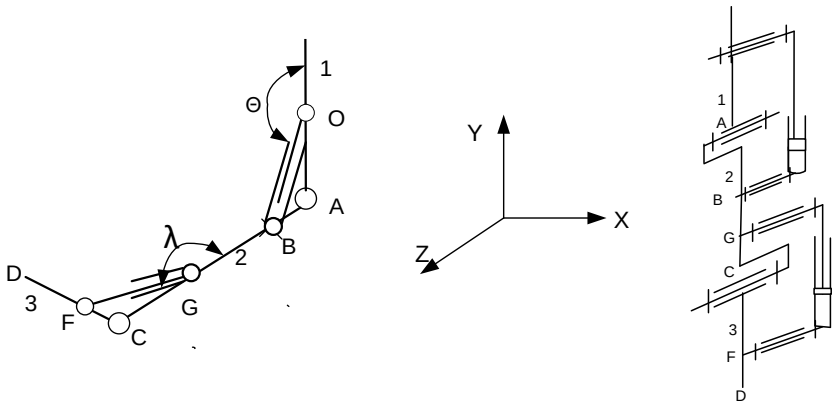

Fig. 16 – Forearm model.

Discretizing the ascending and descending angular movement of the forearm in relation to the humerus (Fig. 14) in k = [0…34] distinct positions, the characteristic parameters of various anatomical elements are obtained.

The variation of the ϕ angle (Fig. 17) is obtained by logical relation (1)

$$\phi_k := \text{if}\left[k \le 17, k \cdot \frac{\pi}{18}, (34 - k) \cdot \frac{\pi}{18}\right] \quad (1)$$

The angular ψ ascending and descending motion of the palm, relative to the forearm (Fig. 14), is discretized in j = [0…20] distinct positions by logical instruction (2) and is shown in Fig. 18.

$$\psi_j := \text{if}\left[j \le 10, \frac{\pi}{2} + j \cdot \frac{\pi}{36}, \frac{\pi}{2} + 10 \cdot \frac{\pi}{36} - (j - 10) \cdot \frac{\pi}{36}\right] \quad (2)$$

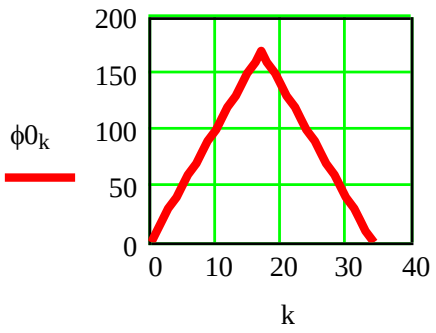

Fig. 17 – The ϕ angle variation.

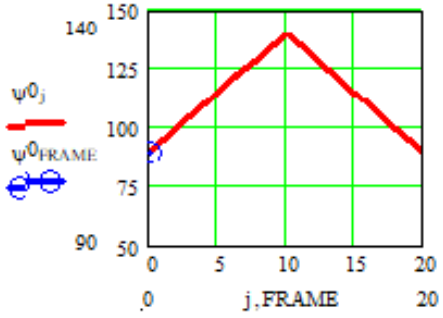

Fig. 18 – The ψ angle variation.

The angular amplitude expressed in degrees is $\Delta\psi = 50^0$.

3. SAGITTAL MODEL ALGORITHM

The modeling of the mechanism in the sagittal plane (Fig. 13 and Fig. 16), is rendered by the algorithm in Mathcad presented in Table 2, which uses the positional-kinematic calculation modules given in other papers [1, 4–8]. The main parameters are used for their graphical vision.

For a variation of the ϕ angle (Fig. 17) of the forearm with an oscillation of 170^0, the trajectories of the kinematic pairs B, C and G are obtained (Fig. 19).

Table 2
Sagittal model algorithm

Algorithm of mechanism modeling in the sagittal plane	
1.	$k := 0..34$
2.	$\phi_k := \text{if}\left[k \le 17, k \cdot \frac{\pi}{18}, (34-k)\cdot\frac{\pi}{18}\right] \quad \phi 0_k := \phi_k \cdot \frac{180}{\pi} \quad \Delta\phi := \max(\phi 0) - \min(\phi 0)$
3.	$XB_k := XA + \left(\frac{-LH}{1.61} + LH\right)\cdot\cos\left(3\cdot\frac{\pi}{2} - \phi_k\right)$ $YB_k := YA + \left(\frac{-LH}{1.61} + LH\right)\cdot\sin\left(3\cdot\frac{\pi}{2} - \phi_k\right)$
4.	$OB_k := \sqrt{(XB_k - XO)^2 + (YB_k - YO)^2}$
5.	$\theta_k := \text{atan}\left(\frac{YB_k - YO}{XB_k - XO}\right) + \pi \;;\; \theta 0_k := \theta_k \cdot \frac{180}{\pi} \;;\; \Delta\theta := \max(\theta 0) - \min(\theta 0)$
6.	$XC_k := XA + LH\cdot\cos\left(3\cdot\frac{\pi}{2} - \phi_k\right) \quad YC_k := YA + LH\cdot\sin\left(3\cdot\frac{\pi}{2} - \phi_k\right)$ $AC_k := \sqrt{(XC_k - XA)^2 + (YC_k - YA)^2}$
7.	$i := 0..8$ $XM_{k,i} := XA + i\cdot\frac{LH}{8}\cdot\cos\left(3\cdot\frac{\pi}{2} - \phi_k\right) \quad YM_{k,i} := YA + i\cdot\frac{LH}{8}\cdot\sin\left(3\cdot\frac{\pi}{2} - \phi_k\right)$
8.	$j := 0..20$
9.	$\psi_j := \text{if}\left[j \le 10, \frac{\pi}{2} + j\cdot\frac{\pi}{36}, \frac{\pi}{2} + 10\cdot\frac{\pi}{36} - (j-10)\cdot\frac{\pi}{36}\right] \quad \psi 0_j := \psi_j \cdot \frac{180}{\pi}$ $\Delta\psi := \max(\psi 0) - \min(\psi 0)$
10.	$XD_{k,j} := XC_k + j\cdot CD\cdot\cos(\psi_j) \quad YD_{k,j} := YC_k + j\cdot CD\cdot\sin(\psi_j)$
11.	$XG_k := XA + AG\cdot\cos\left(3\cdot\frac{\pi}{2} - \phi_k\right) \quad YG_k := YA + AG\cdot\sin\left(3\cdot\frac{\pi}{2} - \phi_k\right)$
12.	$XF_{k,j} := XC_k + j\cdot CF\cdot\cos(\psi_j) \quad YF_{k,j} := YC_k + j\cdot CF\cdot\sin(\psi_j)$
13.	$GF_{k,j} := \sqrt{(YG_k - YF_{k,j})^2 + (XG_k - XF_{k,j})^2}$
14.	$\lambda_{k,j} := \text{atan}\left(\frac{YF_{k,j} - YG_k}{XF_{k,j} - XG_k}\right) \quad \lambda 0_{k,j} := \lambda_{k,j}\cdot\frac{180}{\pi} + 180$ $\Delta\lambda := \max(\lambda 0) - \min(\lambda 0)$

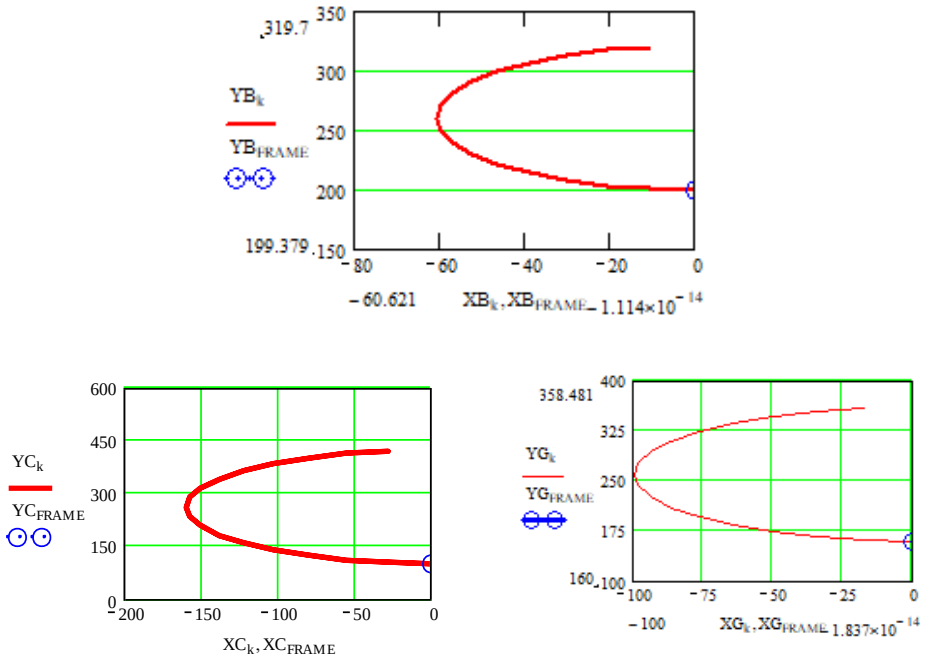

Fig. 19 – Forearm sagittal model characteristics for points B, C and G.

The RTRR module (1,2,4,5) has the OB as independent parameters (Fig. 16), which for a variation of the ϕ angle (Fig. 17) has the values given in Fig. 20 and the angular characteristics θ (Fig. 21), shown (in degrees as θ) with its variation $\Delta\theta = 88.37^0$.

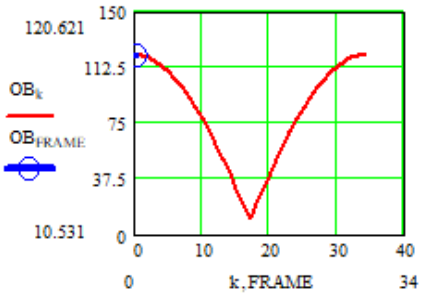

Fig. 20 – Linear parameter OB.

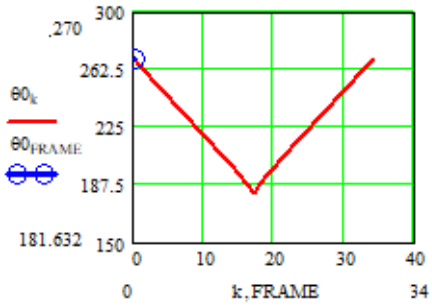

Fig. 21 – Angular parameter θ.

The kinematic pair C connects the element 3 of the mechanism, which simulates the palm (Fig. 17).

The trajectory of the C pair and forearm rendered by $M_i(X_i,Y_i)$ points i = [0…8] for the k discrete angular positions respect to the humerus is shown in Fig. 22.

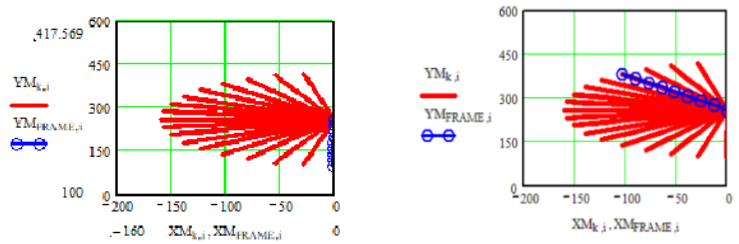

Fig. 22 – The trajectory of the C pair.

Similarly, the tip hand D trajectory (Fig. 23) and the F pair trajectory placed on element 3 (Fig. 24) are represented.

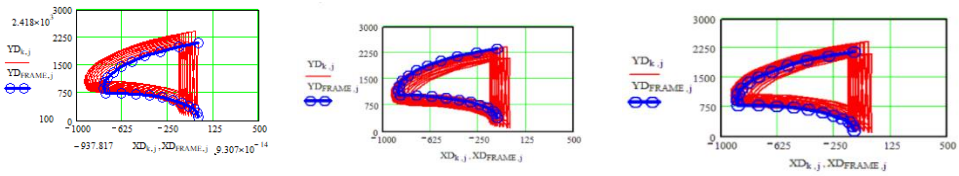

Fig. 23 – Trajectory of D point, tip of the hand.

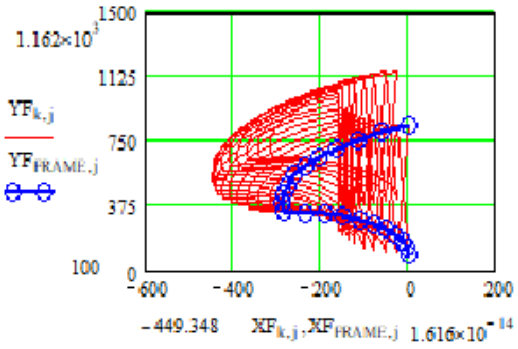

Fig. 24 – Trajectory of F pair.

The RTRR modulus (2, 3, 6, 7) has the GF as independent parameter, which for a variation of the ψ angle (Fig. 18) has the angular characteristic λ (Fig. 16), shown (in degrees as λ) in Fig. 25 for the k – the angular positions of the ulna, and j – the relative angular positions of the palm relative to the forearm, the maximum variation being $\Delta\lambda \cong 179^0$.

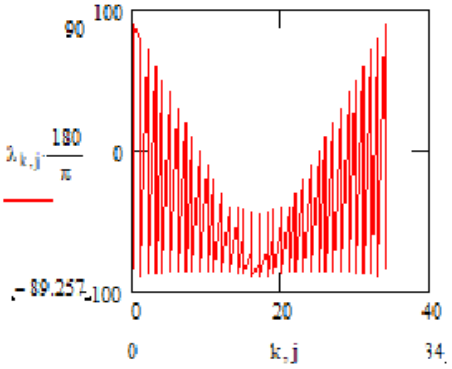

Fig. 25 – λ angle variation.

The model of the arm in the sagittal plane (Fig. 16) can be completed by an RTRR module (10, 11, 12) with a degree of mobility placed in the ZOY plane (Fig. 26) and which gives the palm a rotation around the OX axis perpendicular to the plane of motion.

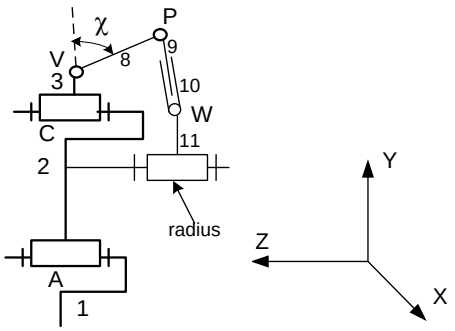

Fig. 26 – The forearm mechanism.

The palm to which the RTRR module belongs (9, 10, 11) may oscillate relative to the OY axis (Fig. 26) with the angle χ (expressed in degrees) by *p*: = 0…10 discrete positions (Fig. 27), which satisfy the logical instruction

$$\chi_p := \text{if}\left[p \le 5, \frac{\pi}{2} + p \cdot \frac{\pi}{36}, \left[\frac{\pi}{2} + 5 \cdot \frac{\pi}{36} + (5 - p) \cdot \frac{\pi}{36}\right]\right] \tag{3}$$

$$\chi 0_p := \chi_p \cdot \frac{180}{\pi}$$

Fig. 27 – χ angle variation.

For *k* relative positions of the ulna in relation to the humerus (Fig. 16), the following parameters (Table 3) are considered for the RTRR module (9, 10, 11) according to its angular position *p* in relation to the OY axis.

Table 3

RTRR (9, 10, 11) algorithm

1.	$XV_k := XC_k \qquad YV_k := YC_k \qquad ZV_k := 0$
2.	$XP_{k,p} := XV_k \qquad YP_{k,p} := YV_k + VP \cdot \cos(\chi_p) \qquad ZP_{k,p} := ZV_k + VP \cdot \sin(\chi_p)$
3.	$XW_{k,p} := XC_k \qquad YW_{k,p} := YC_k \qquad ZW_{k,p} := -30$
4.	$WP_{k,p} := \sqrt{(YP_{k,p} - YW_{k,p})^2 + (ZP_{k,p} - ZW_{k,p})^2}$

Thus, the trajectory of the P pair (Fig. 26), for various *k* positions of the forearm relative to the humerus, is shown in Fig. 28.

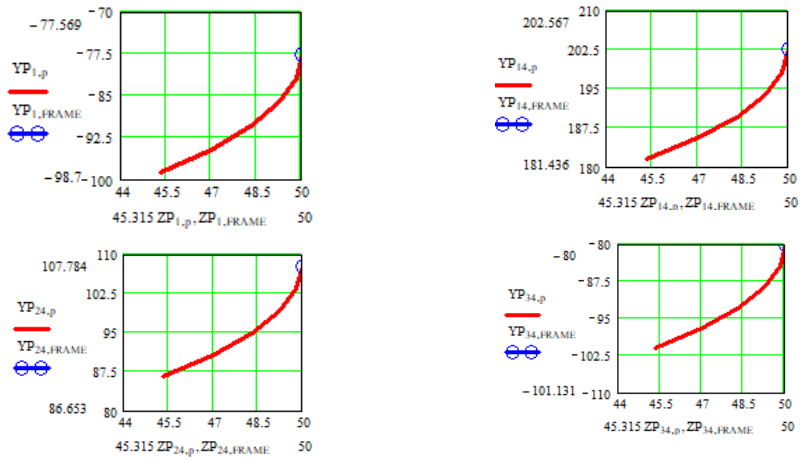

Fig. 28 – P pair trajectory.

The independent parameter $WP_{k,p}$ of the RTRR module (9, 10, 11) causing the palm to oscillate with χ angle (Fig. 27) is the same for any position *k* of the ulna (Fig. 29).

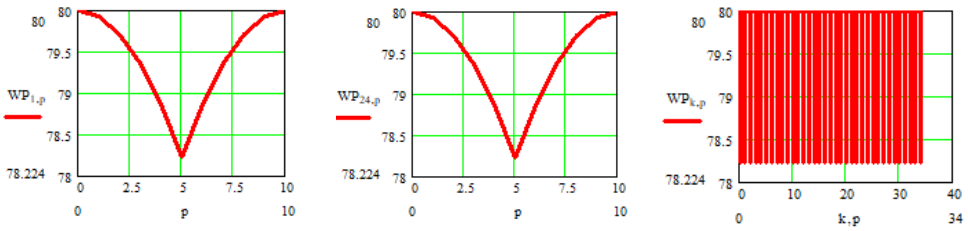

Fig. 29 – $WP_{k,p}$ independent parameter.

4. FOREARM FUNCTIONAL MODELS

The forearm sagittal model with its anatomical data may be completed to ensure pronation-supination movement. For this purpose, the R3$ mechanism is proposed and shown in Fig. 30.

Fig. 30 – Pronation-supination model.

The final structural model mechanism (Fig. 31) includes the elbow joint towards the humerus and the forearm joint with the palm, the spatial mechanism having rotation pairs R, cylindrical C and spherical S pairs.

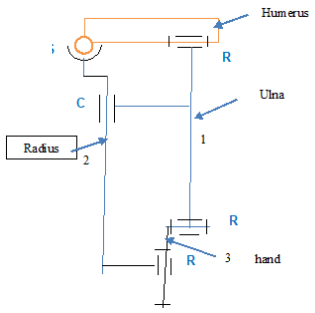

Fig. 31– Forearm spatial mechanism.

An optimized solution is proposed to be used for the construction of the functional system of patients' medical recovery (Fig. 32).

The dimensional characteristics of the rehabilitation mechanism are adopted considering the anatomical data and proportions of human body.

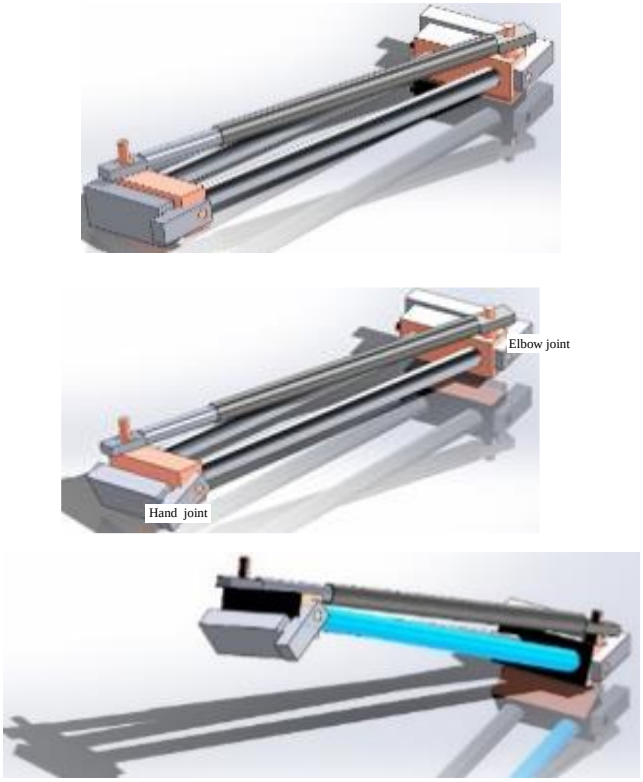

Fig. 32– Forearm model.

5. CONCLUSIONS

The authors of this work (engineers, doctors and therapist) have selected in its first part some important anatomical details of the human upper limb [11–18], which can be sources of inspiration for new solutions of recovery systems slightly addressed in the literature.

The work continues our previous concerns about creating human limb rehabilitation systems, one of the approaches being reproduced in the paper *Multifunctional Medical Recovery and Monitoring System for the Human Lower Limbs*, Sensors Journal, **19,** *22*, Article Number: 5042, doi: 10.3390/s19225042, Published: Nov. 2019, PubMed ID: 31752371, e ISSN: 1424-8220, WOS:000503381500220, 2018 Impact factor 3.031, 2019 (COMANESCU, ADR., DUGAESESCU, I., BOBLEA, D., UNGUREANU, L.).

The field is really fascinating. The upper human limb, as well as the lower one, is a set of bio-mechanisms with open and closed contours, which confer an impressive number of degrees of mobility. This developed aspect can also be a research side. Looking strictly only at the fingers of one hand, simply, each having four active rotation pairs, which can act alone or simultaneously with 2, 3 or 4 others, it results that a single finger can present 15 degrees of mobility, that is

$$\sum_{1}^{4} C_4^i .$$

Also, the five fingers can be moved individually, but also 2, 3, 4, 5 each, resulting in 31 possibilities from

$$\sum_{1}^{5} C_5^i .$$

From the above, it follows that the fingers alone confer a number of 15×31 = 465 degrees of mobility. A careful analysis also deserves the higher pairs of the carpal bones that give additional mobility to the system.

The paper presents some novel mechanisms convering the most important functions of the human forearm and which can be integrated into recovery and monitoring systems.

A first mechanism is a sagittal model of the 2R-2(RTR) arm with specific standard geometric parameters for which a positional calculation algorithm reveals the characteristics of various elements depending on the angular variation of the segments.

It is completed with an R-RTR structure that emphasizes the movement of the palm in the plane perpendicular to the sagittal one in relation to the forearm.

A spatial structure, which reproduces the pronation-supination movement of the forearm is also included.

Finally, a model of the forearm is rendered in connection with the humerus and the palm.

All these models may constitute structures for recovery and monitoring systems.

Received on September, 2024

REFERENCES

1. ANGELES, J., *Fundamentals of Robotic Mechanical Systems: Theory, Methods and Algorithms*, Springer-Verlag, N. York, 2003.
2. MANOLESCU, N. I., *A Unified Method for the Formation of all Planar Jointed Kinematic Chains and Baranov Trusses*, Environment and Planning B, **6**, *4*, pp. 447–454, 1979.
3. MANOLESCU, N. I., *A Method Based on Baranov Trusses, and Using Graph Theory to Find the Set of Planar Jointed Kinematic Chains and Mechanisms*, Mech. Mach. Theory, **8**, *1*, pp. 3–22, 1973.
4. COMANESCU, A., DUGAESESCU, I., BOBLEA, D., UNGUREANU, L., *Multifunctional Medical Recovery and Monitoring System for the Human Lower Limbs*, Sensors Journal, **19,** *22*, Article Number: 5042, DOI: 10.3390/s19225042, Published: Nov. 2019, PubMed ID: 31752371, eISSN: 1424-8220, WOS:000503381500220, 2018 Impact factor 3.031, 2019.
5. COMANESCU, A., COMANESCU, D. & col., *Mechanisms – Analysis and Synthesis – Modelling, Simulation and Optimization of Mechaniical Systems*, Politehnica Press, Bucharest, ISBN:978-606-515-948-8, 2021.
6. COMANESCU, A., BANICA, E., COMANESCU, D., *Human inferior member model for a medical functional recovering system*, 8th World Congress of Biomechanics, 8–12 July 2018, Dublin, Ireland, 2018.
7. COMANESCU, A., BANICA, E., COMANESCU, D., *Leg Mechanisms Motion Characteristics*, Mechanisms, Transmissions and Applications, Proceedings of the Fourth MeTrApp, Conference 2017, pp. 56–66, © Springer International Publishing AG 2018, Mechanisms and Machine Science, ISSN: 2211-0984, ISSN: 2211-0992 (electronic), ISBN: 978-3-319-60701-6, ISBN: 978-3-319-60702-3 (eBook), DOI 10.1007/978-3-319-60702-3, 2017.
8. COMANESCU, A., ZALESCHI. C., *Bi-mobile mechanisms designed by means of their inverse models*, International Conference on Applied Mechanics Electronics and Mechatronics Engineering (AMEME2016), May 28–29, 2016, Beijing, China, pp. 279–285.
9. COMANESCU, A., COMANESCU, D., DUGAESESCU, I., UNGUREANU, L., *Bi-Mobile Leg Mechanism Dynamic Model*, International Conference on Cyber Systems in All Fields of the Life Aerospace, Robotics, Mechanical Engineering, Manufacturing Systems, Biomechatronics, Neurorehabilitation and Human Motricities (ICMERA 2015), Applied Mechanics and Materials, **811**, pp. 273–278, 2015.
10. SECARA, C., CHIROIU, V., DUMITRIU, D., *Obstacle avoidance by a laboratory model of redundant manipulator using a genetic algorithm based strategy*, Proceedings of IV-th National Conference "The Academic Days" of the Academy of Technical Sciences in Romania, November 19–20, 2009, Iassy, AGIR Publishing House, pp. 199–204, 2009.
11. https://emea.search.yahoo.com/search?ei=UTF-8&fr=crmas&p=human+upper+limb.

12. MOREL, W, *3D modelling of the human upper limb including the biomechanics of joints, muscles and soft tissues*, Phd Thesis, Ecole Politechnique, Lausanne, 1999.
13. WEBSTER, J. B., MURPHY. D. P., *Atlas of orthoses and assistive devices*, 5th Edition, Hardback ISBN: 9780323483230, 2018.
14. WANG, H., GUO, J,, PEI, S., WANG, J., YAO, Y., *Upper limb modeling and motion extraction based on multi-space-fusion*, Scientific Reports, Vol. 13, Article number: 16101, www. nature.com/scientificreports, 2023.
15. DE OLIVEIRA, A. C., SULZER, J. S., DESHPANDE, A. D., *Assessment of upper-extremity joint angles using harmony exoskeleton*, IEEE Trans. Neural Syst. Rehabil. Eng. **29**, pp. 916–925, 2021.
16. ZEIAEE, A., ZARRIN, R. S., EIB, A., LANGARI, R., TAFRESHI, R., *A lightweight and compact exoskeleton for upper-limb rehabilitation*, IEEE Robot. Autom. Lett., **7**, *2*, pp. 1880–1887, 2022.
17. SETH, A., MATIAS, R., VELOSO, A. P., DELP, S. L. *A biomechanical model of the scapulothoracic joint to accurately capture scapular kinematics during shoulder movements*, PLoS ONE 11, e0141028, 2016.
18. SETH, A., DONG, M., MATIAS, R., DELP, S. L., *Muscle contributions to upper-extremity movement and work from a musculoskeletal model of the human shoulder*, Front. Neurorobot, **13**, *90*, 2019.
19. DA GAMA, A., E., F., CHAVES, TD., M., FALLAVOLLITA, P., FIGUEIREDO, L. S., TEICHRIEB, V., *Rehabilitation motion recognition based on the international biomechanical standards*, Expert Syst. Appl., 116, pp. 396–409, 2019.
20. WALMSLEY, C. P., *Measurement of upper limb range of motion using wearable sensors*: *A Systematic Review*, Sports Med. Open., **4**, pp. 1–22, 2018.